Current Biology, Vol. 15, 667–671, April 12, 2005, ©2005 Elsevier Ltd All rights reserved. DOI 10.1016/j.cub.2005.02.050

Defective Skeletogenesis with Kidney Stone Formation in Dwarf Zebrafish Mutant for *trpm7*

Michael R. Elizondo,[1,4] Brigitte L. Arduini,[2] Jennifer Paulsen,[3] Erin L. MacDonald,[1] Jaime L. Sabel,[3] Paul D. Henion,[2,*] Robert A. Cornell,[3,*] and David M. Parichy[1,4,*]
[1]Section of Integrative Biology and
Section of Molecular, Cell and Developmental Biology
Institute for Cellular and Molecular Biology
University of Texas at Austin
1 University Station C0930
Austin, Texas 78712
[2]Center for Molecular Neurobiology and
Department of Neuroscience
Ohio State University
105 Rightmire Hall, 1060 Carmack Rd.
Columbus, Ohio 43210
[3]Department of Anatomy and Cell Biology
Roy and Lucille Carver College of Medicine
1-532 Bowen Science Building
University of Iowa
Iowa City, Iowa 52242

Summary

Development of the adult form requires coordinated growth and patterning of multiple traits in response to local gene activity as well as to global endocrine and physiological effectors. An excellent example of such coordination is the skeleton. Skeletal development depends on the differentiation and morphogenesis of multiple cell types to generate elements with distinct forms and functions throughout the body [1–3]. We show that zebrafish *touchtone/nutria* mutants exhibit severe growth retardation and gross alterations in skeletal development in addition to embryonic melanophore and touch-response defects [4, 5]. These alterations include accelerated endochondral ossification but delayed intramembranous ossification, as well as skeletal deformities. We show that the *touchtone/nutria* phenotype results from mutations in *trpm7*, which encodes a transient receptor potential (TRP) family member that functions as both a cation channel and kinase. We find *trpm7* expression in the mesonephric kidney and show that mutants develop kidney stones, indicating renal dysfunction. These results identify a requirement for *trpm7* in growth and skeletogenesis and highlight the potential of forward genetic approaches to uncover physiological mechanisms contributing to the development of adult form.

Results and Discussion

Genetic screens for ethyl-*N*-nitrosourea-induced mutations affecting zebrafish postembryonic development uncovered the *nutria*^{j124e2} mutant, named for its small size, odd shape, and tendency to swim near the surface (Figures 1A and 1B). As embryos and early larvae (2–5 days post fertilization [dpf]), *nutria* are comparable in size to wild-type siblings, but during later development they exhibit a severe growth deficit (Figure 1C). Craniofacial and trunk body proportions are altered, although other external features (e.g., scales, fins, and the complement of adult pigment cells) are not grossly abnormal. To identify the locus causing this dwarf phenotype, we mapped the *nutria* mutation to chromosome 18 in the vicinity of *touchtone* (*tct*) [4, 5]. Both *tct* and *nutria* mutants exhibit embryonic melanophore deficiencies and touch unresponsiveness prior to hatching. Complementation tests confirmed that *nutria* and *tct* are allelic. Fine mapping of the critical region revealed, among other genes, *trpm7*, which encodes an ortholog of the transient receptor potential (TRP) melastatin-7 dual-function cation channel and kinase (0/2889 recombinants) [6]. Although *TRPM7* has not been implicated in growth previously, a member of this family, *TRPM1* (*melastatin*), is expressed in human melanocytic nevi [7], and zebrafish melanophores require *tct* cell autonomously [4, 5].

Our data show that *trpm7* corresponds to *tct*. Sequencing *trpm7* cDNAs revealed premature stop codons in the severe alleles *tct*^{j124e1} and *tct*^{b508} (see the Supplemental Data available with this article online). Moreover, the injection of wild-type embryos with a *trpm7* splice-blocking morpholino oligonucleotide results in both melanophore deficiencies and touch unresponsiveness and thus phenocopies the mutant (see Supplemental Data). Finally, TRPM7 acts as an inwardly rectifying cation channel with broad specificity but high affinity for Mg^{2+} and Ca^{2+}, suggesting that manipulating divalent-cation availability might rescue embryonic phenotypes of *trpm7* mutants [8, 9]. Supplemental Mg^{2+} partially rescued melanophore development, whereas supplemental Ca^{2+} partially rescued melanophore development and touch responsiveness (Figures 1D–1F; Supplemental Data). Thus, *trpm7* is the gene affected in *tct* mutants.

To clarify the mode(s) of *trpm7* activity, we examined *trpm7* expression in wild-type embryos and larvae. Consistent with previous observations, we detected widespread *trpm7* expression at embryonic stages, including in the central nervous system, pronephros, lens, and other tissues [10] (data not shown). In metamorphic larvae, transcripts were abundant in liver, mesonephric kidney tubules, and corpuscles of Stannius, which are teleost glands that contribute to calcium homeostasis [11] (Figures 2A–2C). In contrast to severe alleles, *trpm7*^{j124e2} (*nutria*) individuals are viable, allowing us to assess functional consequences of *trpm7* mutation during postembryonic development. Consistent with kidney expression of *trpm7*, histological examination of *trpm7*^{j124e2} mutant larvae revealed mineralization within mesonephric tubules (Figures 2D and 2F). These data suggest that altered *trpm7* function in the kidney, in corpuscles of Stannius, or in both af-

*Correspondence: henion.1@osu.edu (P.H.); robert-cornell@uiowa.edu (R.C.); dparichy@u.washington.edu (D.P.)
[4]Present address: Department of Biology, University of Washington, Box 351800, Seattle, Washington 98195.

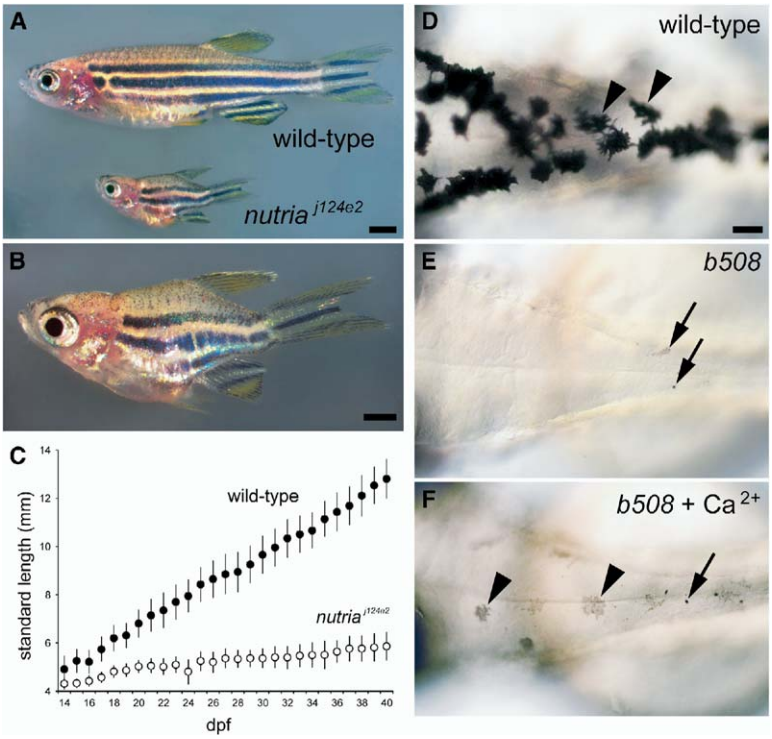

Figure 1. Retarded Growth and Altered Body Proportions in *nutria* (*tct*) Mutant Zebrafish with Embryonic Melanophore Defect Rescuable by Divalent-Cation Supplementation

(A) Wild-type and *nutria* siblings, 50 dpf.

(B) Higher-magnification image of a *nutria* mutant.

(C) Diminished growth of *nutria* compared to wild-type siblings. Each point shows the mean standard length ± standard deviation for seven to 20 individuals.

(D–F) Embryonic melanophore defects are rescuable with supplemental Ca^{2+}. (D) Wild-type embryos exhibit well-melanized and well-spread melanophores (arrowheads). (E) Mutants exhibit few poorly melanized and punctate melanophores or melanophore fragments (arrows); tct^{b508} is shown. (F) In a medium supplemented with Ca^{2+}, mutant melanophores are more numerous, spread, and melanized (arrowheads), although some punctate melanophores remain (arrow).

Scale bars represent the following: (A), 2 mm; (B), 1 mm; (D–F), 100 μm.

fects whole-organism cation homeostasis and leads to nephrolithiasis.

Because dwarfism syndromes in humans are associated with a range of skeletal defects [12] and cation homeostasis affects bone development and maintenance [13], we asked whether the growth deficit and disproportionality of $trpm7^{j124e2}$ mutants is associated with changes in ossification. A comprehensive analysis of 87 bones between 9 and 51 dpf revealed extensive alterations in ossification sequence between wild-type and mutant larvae (Figures 3 and 4). Among numerous examples of sequence reordering is the epural bone of the caudal fin, which is the 78th bone to ossify in wild-type larvae but only the 32nd to ossify in *trpm7* mutant larvae. Conversely, the maxilla is the 15th bone to ossify in wild-type larvae but the 40th to ossify in *trpm7* mutant larvae. Thus, $trpm7^{+}$ is essential for the normal sequence of ossification.

To better understand ossification changes, we categorized bones according to function and anatomical location as well as cellular origin. The most dramatic differences were between endochondral bones, which develop through mineralization of a cartilage model, and intramembranous bones, which develop directly, without a cartilage model [1, 14, 15]. In *trpm7* mutants, endochondral bones (red connectors in Figure 4A) appeared on average earlier in the ossification sequence than they did in wild-type larvae, whereas intramembranous bones (green connectors) appeared on average later than they did in wild-type larvae. Dissociation of endochondral and intramembranous ossification is exemplified by the caudal complex, in which the endochondral hypurals and epural ossify much earlier in *trpm7* mutants compared to the wild-type, whereas the intramembranous urostyle, centra, and other bones ossify much later in *trpm7* mutants compared to the wild-type (Figures 3A–3H). Precocious endochondral ossification is similarly evident in the suspensorium and the branchial arches of *trpm7* mutants (Figures 3I–3P), whereas delayed intramembranous ossification is apparent for several bones of the anterior head (Figures 3Q–3V). The accelerated ossification of endochondral bones and the delayed ossification of intramembranous bones reflect order in the ossification sequence as well as absolute timing. One can most easily visualize these timing differences by plotting how genotype affects the likelihood of bones being ossified at any given age against the statistical significance of these differences (Figures 4B and 4C). Defects in ossification timing do not simply reflect growth retardation; even severely runted wild-type fish develop skeletal elements of normal shape without premature ossification (Supplemental Data).

Furthermore, functional-anatomical units in close proximity were found to be differentially affected, even after we controlled for the relative contributions of endochondral and intramembranous bones within these units. For example, otic bones are accelerated, whereas orbital bones are delayed, despite the anatomical proximity of these bones and their similar endochondral and intramembranous compositions (Figure 4C; Table S1). Finally, *trpm7* mutants exhibited skeletal dysplasia, including extreme malformation of the Weberian (auditory) apparatus and the ribs, compressed vertebrae (of normal number), and kinks in the posterior vertebral column (Figures 3D, 3H, 3S, and 3W).

We have demonstrated that *trpm7* is essential for growth and skeletogenesis during the zebrafish larval-

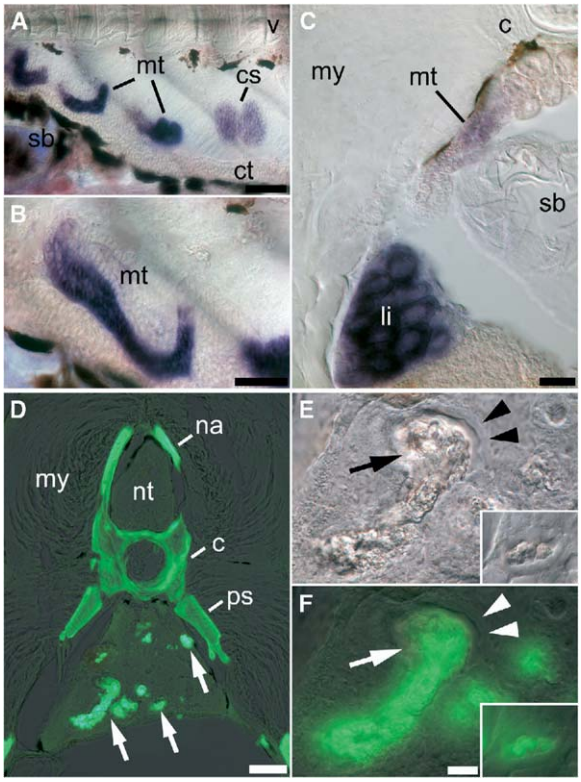

Figure 2. *trpm7* Expression in Wild-Type Larvae and Kidney Stone Formation in *trpm7* Mutants

(A–C) *trpm7* expression in metamorphosing wild-type larvae. (A) At early stages of metamorphosis (14 dpf), *trpm7* mRNA is present in mesonephric tubules (mt) and corpuscles of Stannius (cs). The following abbreviations are used: v, vertebral column; sb, swimbladder; and ct, mesonephric collecting tubule. *trpm7* expression is also detectable in more-anterior regions of the mesonephros (not shown). (B) A higher-magnification *trpm7*$^{+}$ mesonephric tubule is shown. (C) Transverse section of late-metamorphic (24 dpf) larva. *trpm7* transcripts are present in mesonephric tubules and liver (indicated by "li"). *trpm7* transcripts are not detectable in developing endochondral or intramembranous bones. "my" denotes myotome and "c" denotes centrum.

(D–F) *trpm7*^{j124e2} (*nutria*) mutants develop kidney stones. (D) Calcein staining reveals skeletal elements (na, c, ps) and ectopic mineralization (arrows). The following abbreviations are used: na, neural arches; c, centrum; ps, pleural spines; and nt, neural tube. (E) shows left-most ectopic mineralization from panel (D). Epithelium (arrowheads) surrounds the mineralized deposit (arrow). The inset shows mineralized deposit within collecting tubule of another larva. (F) shows calcein staining of mineralized deposits shown in panel (E) and the inset.

Scale bars represent the following: (A), 60 μm; (B), 40 μm; (C) and (D), 80 μm; (E) and (F), 20 μm (15 μm for insets).

to-adult transition and for melanophore development and touch response during embryogenesis. *trpm7* expression in kidney and corpuscles of Stannius, as well as the presence of kidney stones in *trpm7* mutants, support a model in which effects on growth and skeletogenesis reflect physiological regulation of cation homeostasis. These effects may be analogous to those of parathyroid hormone/parathyroid hormone receptor type 1 (PTHR1) regulation of calcium homeostasis in mammals, in which changes in PTHR1 signaling or downstream effectors such as Runx2 can lead to premature endochondral ossification [16–19]. However, this model does not readily explain the delayed intramembranous ossification observed in *trpm7* mutants. Although the precise functions of *trpm7* in promoting normal ossification sequence and timing, as well as melanophore development and touch response, remain to be elucidated, our analyses reveal important roles for *trpm7* in the physiological regulation of postembryonic growth and skeletogenesis.

Supplemental Data

Supplemental Data, including four figures, Supplemental Experimental Procedures, and a table, can be found with this article online at http://www.current-biology.com/cgi/content/full/15/7/667/DC1/.

Acknowledgments

The authors thank S.L. Johnson for providing *trpm7*^{j124e1} and *trpm7*^{j124e2}, T. Juenger and T. Wilcox for discussion of analytical methods, J. Wallingford for comments on the manuscript, and C. Lee for help rearing fish. We gratefully acknowledge embryonic *trpm7* expression data provided online by Thisse, B., Pflumio, S., Fürthauer, M., Loppin, B., Heyer, V., Degrave, A., Woehl, R., Lux, A., Steffan, T., Charbonnier, X.Q., and Thisse, C. (Expression of the zebrafish genome during embryogenesis, 2001, National Institutes of Health R01 RR15402). The authors were supported by National Institutes of Health grants R01 HD40165 and R01 GM62182 (to D.M.P.), R01 GM067841 (to R.A.C.), and R01 NS38115 (to P.D.H.) and by American Cancer Society grant IRG-77-004-25, administered by the University of Iowa, to R.A.C.

Received: December 23, 2004
Revised: January 31, 2005
Accepted: February 16, 2005
Published: April 12, 2005

References

1. Karsenty, G., and Wagner, E.F. (2002). Reaching a genetic and molecular understanding of skeletal development. Dev. Cell *2*, 389–406.
2. Fisher, S., Jagadeeswaran, P., and Halpern, M.E. (2003). Radiographic analysis of zebrafish skeletal defects. Dev. Biol. *264*, 64–76.
3. Kronenberg, H.M. (2003). Developmental regulation of the growth plate. Nature *423*, 332–336.
4. Cornell, R.A., Yemm, E., Bonde, G., Li, W., d'Alencon, C., Wegman, L., Eisen, J., and Zahs, A. (2004). Touchtone promotes survival of embryonic melanophores in zebrafish. Mech. Dev. *121*, 1365–1376.
5. Arduini, B.L., and Henion, P.D. (2004). Melanophore sublineage-specific requirement for zebrafish touchtone during neural crest development. Mech. Dev. *121*, 1353–1364.
6. Wolf, F.I. (2004). TRPM7: Channeling the future of cellular magnesium homeostasis? Sci. STKE *2004*, pe23.
7. Duncan, L.M., Deeds, J., Hunter, J., Shao, J., Holmgren, L.M., Woolf, E.A., Tepper, R.I., and Shyjan, A.W. (1998). Down-regulation of the novel gene melastatin correlates with potential for melanoma metastasis. Cancer Res. *58*, 1515–1520.
8. Monteilh-Zoller, M.K., Hermosura, M.C., Nadler, M.J., Scharenberg, A.M., Penner, R., and Fleig, A. (2003). TRPM7 provides an ion channel mechanism for cellular entry of trace metal ions. J. Gen. Physiol. *121*, 49–60.
9. Schmitz, C., Perraud, A.L., Johnson, C.O., Inabe, K., Smith, M.K., Penner, R., Kurosaki, T., Fleig, A., and Scharenberg, A.M. (2003). Regulation of vertebrate cellular Mg^{2+} homeostasis by TRPM7. Cell *114*, 191–200.

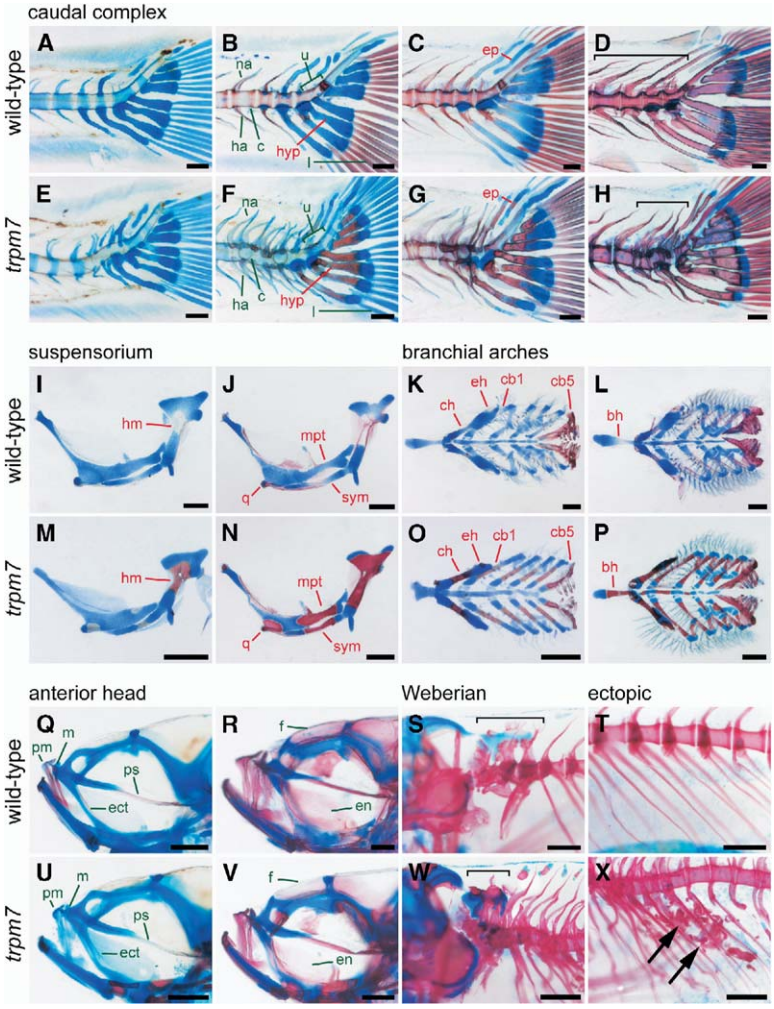

Figure 3. *trpm7*^{i124e2} Mutants Exhibit Dramatic Differences in Skeletal Development in Comparison to Wild-Type

Alizarin red stains ossified bone and mineralized tissues. Alcian blue stains cartilage. Endochondral bone labels are red, and intramembranous bone labels are green.

(A–H) Differences in ossification timing in the caudal complex between wild-type (A–D) and mutant (E–H) siblings (9–44 dpf, left to right). In mutants, endochodondral bones ossify earlier [panels (B) and (F): hyp. Panels (C) and (G): ep], whereas intramembranous bones ossify later [panels (B) and (F): na, u, ha, c, l]. Compression of vertebrae and the caudal complex are evident [panels (D) and (H): brackets].

(I–P) The suspensorium (I–N) and branchial arches (K–P) illustrate precocious endocondral ossification in mutants. Advances in ossification are apparent for several endochondral bones at early stages [17 dpf. Panels (I) and (M): hm. Panels (K) and (O): ch, eh, cb1] and later stages [47 dpf. Panels (J) and (N): mpt, q, sym. Panels (L) and (P): bh].

(Q, U, R, V) Bones of the anterior head illustrate delayed intramembranous ossification in mutants. Intramembranous bones are delayed in mutants at early stages [24 dpf. Panels (Q) and (U): pm, m, ps, ect] and later stages [44 dpf. Panels (R) and (V): f, en].

(S, W) Bones of the Weberian apparatus (brackets) are malformed and compressed in mutants.

(T, X) Mineralizations within the mesonephros of mutant larvae [arrowheads in panel (X)].

(S) and (T) are at 35 dpf; (W) and (X) are at 30 dpf. The following abbreviations are used: bh, basihyal; c, centra; cb1, ceratobranchial 1; cb5, ceratobranchial 5; ch, ceratohyal; ect, ectopterygoid; eh, epihyal; en, entopterygoid; ep, epural; f, frontal; ha, hemal arches; hm, hyomandibula; hyp, hypurals; l, lepidotrichia; m, maxilla; mpt, metapterygoid; na, neural arches; pm, premaxilla; ps, parasphenoid; q, quadrate; sym, symplectic; and u, urostyle and ural 1 + 2.

Scale bars represent the following: (A–H), 100 μm; (I–X), 250 μm.

10. The Zebrafish Information Network. 2005. (http://zfin.org).
11. Krishnamurthy, V.G. (1976). Cytophysiology of corpuscles of Stannius. Int. Rev. Cytol. *46*, 177–249.
12. Hall, C.M. (2002). International nosology and classification of constitutional disorders of bone (2001). Am. J. Med. Genet. *113*, 65–77.
13. Dvorak, M.M., and Riccardi, D. (2004). Ca^{2+} as an extracellular signal in bone. Cell Calcium *35*, 249–255.
14. Cubbage, C.C., and Mabee, P.M. (1996). Development of the cranium and paired fins in the zebrafish *Danio rerio* (ostariophysi, Cyprinidae). J. Morphol. *229*, 121–160.
15. Bird, N.C., and Mabee, P.M. (2003). Developmental morphology of the axial skeleton of the zebrafish, *Danio rerio* (Ostariophysi: Cyprinidae). Dev. Dyn. *228*, 337–357.
16. Schipani, E., Kruse, K., and Juppner, H. (1995). A constitutively active mutant PTH-PTHrP receptor in Jansen-type metaphyseal chondrodysplasia. Science *268*, 98–100.
17. Karaplis, A.C., He, B., Nguyen, M.T., Young, I.D., Semeraro, D., Ozawa, H., and Amizuka, N. (1998). Inactivating mutation in the human parathyroid hormone receptor type 1 gene in Blomstrand chondrodysplasia. Endocrinology *139*, 5255–5258.
18. Takeda, S., Bonnamy, J.P., Owen, M.J., Ducy, P., and Karsenty, G. (2001). Continuous expression of Cbfa1 in nonhypertrophic chondrocytes uncovers its ability to induce hypertrophic chondrocyte differentiation and partially rescues Cbfa1-deficient mice. Genes Dev. *15*, 467–481.
19. Ueta, C., Iwamoto, M., Kanatani, N., Yoshida, C., Liu, Y., Enomoto-Iwamoto, M., Ohmori, T., Enomoto, H., Nakata, K., Takada, K., et al. (2001). Skeletal malformations caused by overexpression of Cbfa1 or its dominant negative form in chondrocytes. J. Cell Biol. *153*, 87–100.

Accession Numbers

The GenBank accession number reported in this paper for *trpm7* is AY860421.

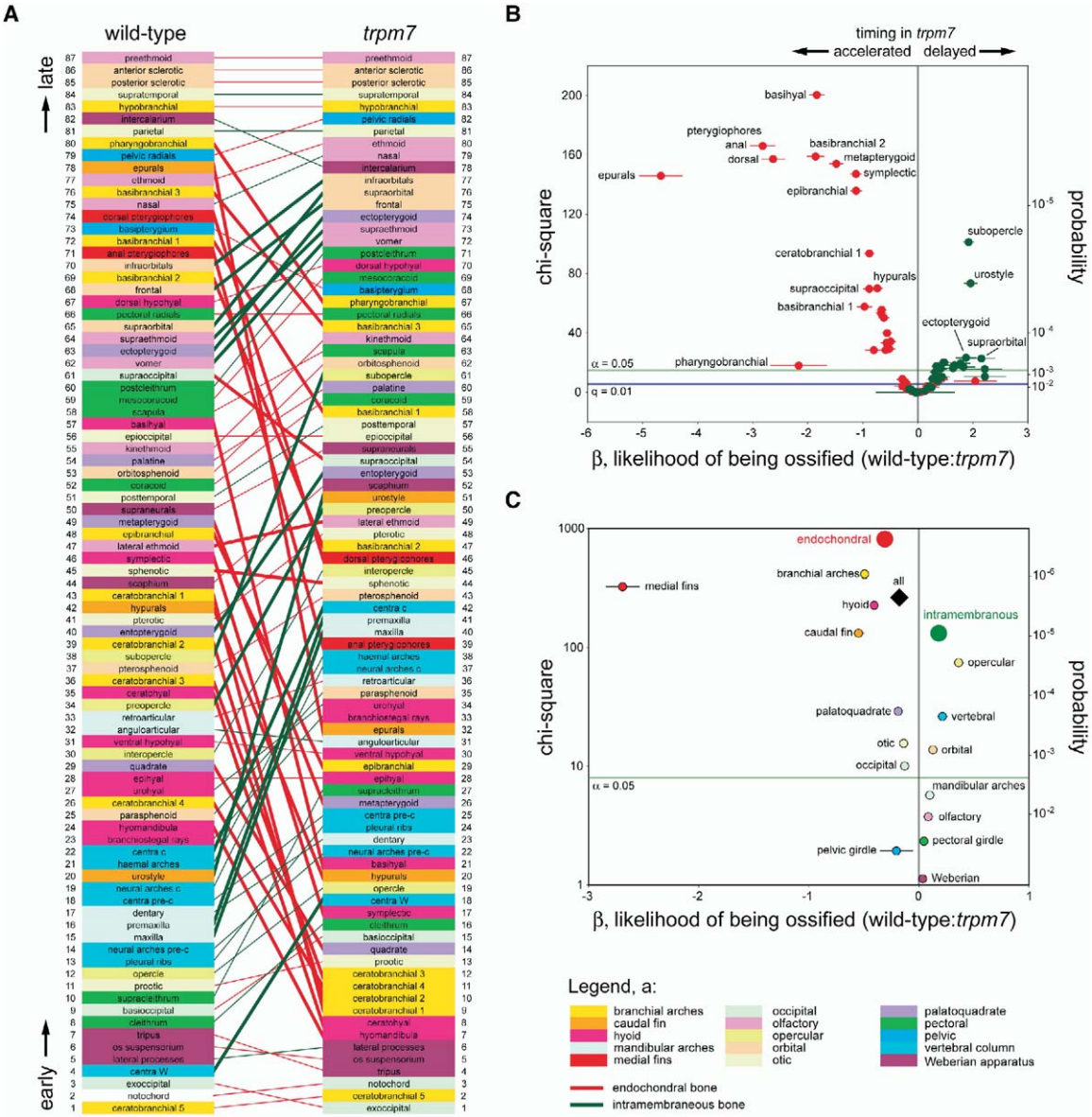

Figure 4. Altered Sequence and Timing of Skeletal Ossification in *trpm7*^{j124e2} Compared to the Wild-Type

Wild-type larvae (*n* = 500) and *trpm7* mutant siblings (*n* = 431) were scored for ossification of 87 bones, yielding 80,997 ossification scores. Schematics of bone locations, functional-anatomical units, and effects for each bone are in the Supplemental Data.

(A) In mutants, endochondral bones (red connectors) appear on average earlier in the ossification sequence, whereas intramembranous bones (green connectors) appear on average later in the ossification sequence. Bold connectors show bones in which ossification timing, in addition to sequence, was significantly altered [panel (B)].

(B) In mutants, analyses by developmental mode reveal accelerated ossification for many endochondral bones (red) but delayed ossification for many intramembranous bones (green). The *x* axis shows the relative likelihood of ossification in the wild-type compared to the mutant: estimates greater than 0 indicate that the bone is more likely to be ossified in wild-type, and ossification is therefore delayed in the mutant; estimates less than 0 indicate that the bone is less likely to be ossified in wild-type fish, and ossification is therefore accelerated in the mutant. The *y* axis shows statistical significance by chi-square value (left axis) and p value (right axis). $\alpha = 0.05$ and q = 0.01 are the thresholds of statistical significance after multiple comparisons were controlled for.

(C) Analyses by functional-anatomical unit and developmental mode. Functional-anatomical units were differentially affected in the mutants even after their relative endochrondral and intramembranous compositions were controlled for. Averages: of all bones, diamond; of endocondral bones, large red point; of intramembranous bones, large green point.

Error bars in (B) and (C) show one standard error for logistic regression coefficients, β.

Supplemental Data

Defective Skeletogenesis with Kidney Stone Formation in Dwarf Zebrafish Mutant for *trpm7*

Michael R. Elizondo, Brigitte L. Arduini, Jennifer Paulsen, Erin L. MacDonald, Jaime L. Sabel, Paul D. Henion, Robert A. Cornell, and David M. Parichy

Supplemental Experimental Procedures

Fish Stocks and Maintenance

Mutations were induced in wild-type AB, SJD, and wik^{ut} genetic backgrounds by standard methods of ethyl-*n*-nitrosourea mutagenesis. Fish were reared at 28.5°C and fed rotifers, paramecia, or dry flake food, as appropriate. For growth series of wild-type fish and *nutria* mutants, fish were reared individually from embryonic through adult stages and fed ad libitum to eliminate competition. For staining series, wild-type and mutant individuals were sorted at 3 dpf and then reared separately at equivalent densities to minimize variation in growth rates within each genotype.

Skeletal Staining and Classification

Fish were fixed in 4% paraformaldehyde in phosphate-buffered saline (PBS) for 48 hr and dehydrated over 2 days to 100% ethanol. They were then stained with Alcian blue for cartilage, digested with trypsin, and stained with Alizarin red for bone according to a standard protocol for fish larvae [S1]. Fish were transferred to 100% glycerol over 1 week for analysis and storage. For calcein staining, we fixed larvae with 4% paraformaldehyde in PBS, embedded them in OCT, and collected cryosections on Fisherbrand Superfrost Plus slides. After they were dried and rinsed in PBS, slides were immersed in 0.1% calcein in PBS for 10 min, rinsed extensively in PBS, and coverslipped. The classification of bones by method of ossification and anatomical-functional units followed that used by references [S2–S4].

Genetic Mapping and Sequencing

Meiotic mapping was performed by standard methods using haploid and diploid mapping panels constructed with AB and wik mapping strains (panel sizes: *trpm7*^{j124e2}, 1400 haploid embryos; *trpm7*^{b722}, 1000 diploid embryos; *trpm7*^{b508}, 435 haploid embryos; and *trpm7*^{b508}, *trpm7*^{os1}, and *trpm7*^{os2}, 54 diploid embryos). For identification of mutant lesions, polymerase chain reaction (PCR) products of *trpm7* cDNAs were sequenced directly and compared with sequences derived from the corresponding unmutagenized genetic background.

Morpholino-Based Gene Knockdown

For morpholino-injection experiments, eggs were obtained from natural matings of wild-type fish of the ZDR strain (Scientific Hatcheries, Huntington Beach, California). Morpholino oligonucleotides (GeneTools, Sumerton, Oregon) were diluted to 20 mg/ml in Danieau buffer and then to 0.8 mg/ml in 0.2 M KCl for injection. We designed a morpholino (GTG TGT GAG ATT TAC TCT GCT GTT C) to interfere with splicing [S5] at the junction between exon 12 and intron 12. Embryos were injected at the 2- to 4-cell stage with approximately 5 nl of 0.8 mg/ml *trpm7* morpholino or of the standard negative control morpholino (GeneTools). Sequencing of morpholino-injected embryos confirmed failed splicing of intron 12, and this failure resulted in a frameshift and a premature stop codon (not shown). With all morpholinos, we observed approximately 5% mortality before 12 hpf, presumably from injection wounds. At all stages, embryos injected with standard negative-control morpholino appeared identical to uninjected embryos (not shown). A phenotype of highly reduced melanophore differentiation throughout the embryo (shown in Figure S1) was observed in 80% of injected embryos ($n = 60$), with other embryos showing a less-pronounced phenotype. Limited morpholino perdurance precluded testing for effects of morpholino knockdown on late-developing kidney and ossification phenotypes.

In Situ Hybridization

Whole-mount in situ hybridization, with minor modifications, followed [S6]. In brief, larvae were fixed over 2 nights in 4% paraformaldehyde and 1% DMSO in PBS, transferred to methanol, and then rehydrated to PBST (PBS with 0.2% Tween-20). Larvae were treated for 30 min with 20 μg/ml proteinase-K in PBST containing 1% DMSO, postfixed for 20 min in 4% paraformaldehyde in PBST, washed in PBST, and then washed three times in a hybridization solution lacking transfer RNA (tRNA) and heparin. Prehybridizations were performed overnight at 68°C in a hybridization solution (50% formamide, 5× SSC, 500 mg/ml yeast tRNA, 50 mg/ml heparin, 0.2% Tween-20, and 9.2 mM citric acid). Hybridizations were performed over two nights at 68°C in a fresh hybridization solution containing antisense digoxygenin-labeled riboprobes fractionated to ~300 nucleotides. Probes derived from 5′ and 3′ ends of *trpm7* transcripts yielded qualitatively similar results. Larvae were then washed twice in 2× SSCT and three times for 2 hr each in 0.2× SSCT at 68°C. After graded changes were made to maleic acid buffer (MAB; 100 mM maleic acid [pH 7.5] and 150 mM NaCl), larvae were blocked overnight with Roche blocking reagent in MAB at 4°C, incubated over 3 nights in a fresh blocking reagent containing 1:5000 anti-digoxygenin alkaline phosphatase-conjugated Fab fragments (Roche), and then washed over 3 additional nights in MAB. Larvae were then transferred to alkaline phosphate buffer (100 mM Tris [pH 9.5], 50 mM $MgCl_2$, 100 mM NaCl, and 0.1% Tween-20), and the color was developed with NBT/BCIP.

Cation Rescue Experiments

tct^{b508} mutant embryos and wild-type siblings were obtained from matings of heterozygous carriers. Chorionated embryos were reared to the 26-somite stage in water and then transferred to embryo medium [S7] (17.9 mM NaCl; "0" in Figure S2) or modified embryo medium (4.2 mM NaCl; "−" in Figure S2) with or without the addition of $MgCl_2$ (100 mM) or $CaCl_2$ (50 mM or 100 mM). We tested touch response by prodding embryos still in their chorions one time with a probe at the midtrunk level; any response to this stimulus was considered a rescue. Melanophore morphologies were examined over the head and trunk; the presence of any well-spread melanophores of normal size was considered a rescue. Both melanophore and touch-response phenotypes were observed between 48 and 60 hpf. Treatments were replicated across multiple families two to seven times with seven to 35 embryos per condition.

Quantitative Analyses of Ossification Sequence and Timing

We reconstructed ossification sequences in wild-type fish and *trpm7* mutants by determining the frequency with which each skeletal element was ossified within all individuals of each genotype and then ordering these frequencies into ranks [S8]. Elements that failed to ossify within the range of ages examined were ordered arbitrarily (ranks 83–87 in Figure 4A in the main text). Differences in rank between wild-type fish and mutants were highly significant between endochondral and intramembranous bones (Wilcoxon test: $Z = 6.03$, d.f. $= 1$, $p < 0.0001$).

To assess likelihoods of bone ossification, we performed separate logistic regression analyses for each bone, developmental mode (endochondral and intramembranous), or functional-anatomical unit with genotype as a main effect and dpf as a covariate. Alternative models, including only genotype or including genotype and other main effects to control for stage and batch variability (e.g., standard length of wild-type siblings), yielded qualitatively similar results. Note that estimates of timing differences between genotypes reflect

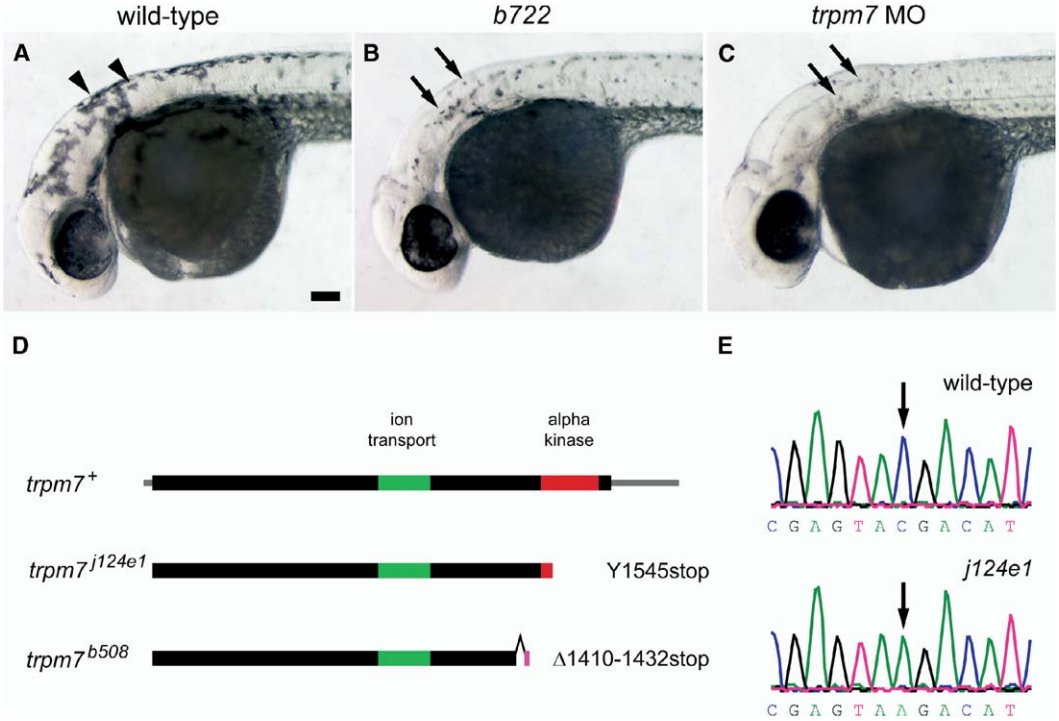

Figure S1. Identification of *trpm7* as the Gene Mutated in *tct* (*nutria*) Mutant Zebrafish

(A–C) Morpholino knockdown of *trpm7* phenocopies the *tct* embryonic melanophore defect. (A) In wild-type embryos, well-melanized and well-spread melanophores (arrowheads) cover the dorsum and head at 48 hr. (B) In *tct* embryos, melanophores are fewer, lighter, and punctate (arrows) [S10, S11]. An allele of moderate severity, tct^{b722}, is shown. (C) Wild-type embryos injected with a splice-blocking morpholino to *trpm7* exhibit fewer, lighter, and punctate melanophores, as in *tct*.

(D) Schematic of *trpm7* cDNAs. Seqencing of *trpm7* cDNAs identifies a transcript encoding at least 1773 amino acids (aa), including an ion-transport domain (aa 873–1073) and an α kinase domain (aa 1510–1724). tct^{j124e1} shows a C→A transversion resulting in substitution of a premature stop codon for tyrosine at aa 1545, near the start of the α kinase domain. Sequencing of tct^{b508} reveals a 68 nucleotide deletion (aa 1410–1432) comprising a single exon and resulting in a frameshift, 16 novel amino acids, and a premature stop codon. Analyses of genomic DNA reveal a deletion corresponding to one exon in addition to parts of flanking introns.

(E) Sequence electropherograms from haploid embryos that are wild-type (upper section) or the strong allele tct^{j124e1} that exhibits a premature stop codon (TAA, lower section). *trpm7* Genbank accession number: AY860421.

Scale bars in (A)–(C) represent 100 μm.

only the onset of ossification as evidenced by the first indication of Alizarin-red staining; they do not account for differences in rate once ossification has started. Overall, *trpm7* mutants exhibited greatly accelerated ossification rates for endochondral bones and correspondingly delayed ossification rates for intramembranous bones even after ossification had commenced. Analyses shown here thus underestimate the magnitude of differences between genotypes. Because of the large numbers of individual tests for logistic regression analyses, we assessed overall significance levels by means of a standard Bonferroni correction ($\alpha = 0.05$, adjusted, critical significance level = 0.000127), which is likely to be overly conservative, as well as a more recent method of assessing false discovery rate (q value) [S9]. We provide both significance thresholds in Figure 4B in the main text. For the smaller number of tests for developmental mode and functional-anatomical units, we provide only the Bonferroni-corrected significance threshold (Figure 4C in the main text). See Table S1 for a complete listing of effects and significance levels by bone. Statistical analyses were performed with JMP 5.0.1a for Apple Macintosh computers (SAS Institute, Cary, NC) and software of [S9].

Supplemental References

S1. Potthoff, T. (1984). Clearing and staining techniques. In Ontogeny and Systematics of Fishes, H.G. Moser, W.J. Richards, D.M. Cohen, M.P. Fahay, A.W. Kendall, Jr., and S.L. Richardson, eds. (Lawrence, Kansas: Special Publication *1*, American Society of Ichthyologists and Herpetologists, Allen Press), pp. 35–37.

S2. Cubbage, C.C., and Mabee, P.M. (1996). Development of the cranium and paired fins in the zebrafish *Danio rerio* (ostariophysi, Cyprinidae). J. Morphol. 229, 121–160.

S3. Bird, N.C., and Mabee, P.M. (2003). Developmental morphology of the axial skeleton of the zebrafish, *Danio rerio* (Ostariophysi: Cyprinidae). Dev. Dyn. 228, 337–357.

S4. Fleming, A., Keynes, R., and Tannahill, D. (2004). A central role for the notochord in vertebral patterning. Development 131, 873–880.

S5. Draper, B.W., Morcos, P.A., and Kimmel, C.B. (2001). Inhibition of zebrafish fgf8 pre-mRNA splicing with morpholino oligos: a quantifiable method for gene knockdown. Genesis 30, 154–156.

S6. Quigley, I.K., Turner, J.M., Nuckels, R.J., Manuel, J.L., Budi, E.H., Macdonald, E.L., and Parichy, D.M. (2004). Pigment pattern evolution by differential deployment of neural crest and post-embryonic melanophore lineages in *Danio* fishes. Development 131, 6053–6069.

S7. Westerfield, M. (2000). The Zebrafish Book: A Guide for the Laboratory Use of Zebrafish (*Danio rerio*), Fourth Edition. (Eugene, Oregon: University of Oregon Press).

S8. Mabee, P.M., Olmstead, K.L., and Cubbage, C.C. (2000). An

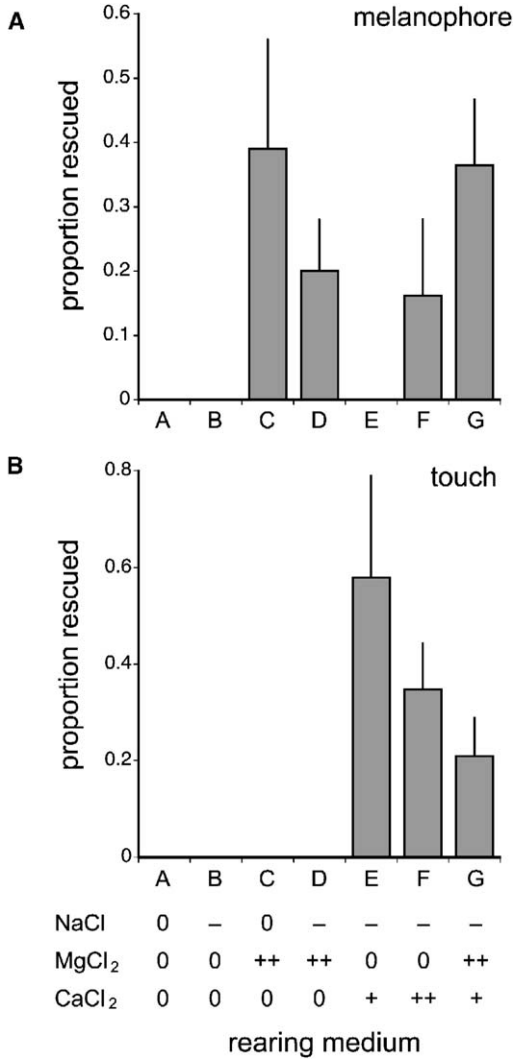

Figure S2. Rescue of *trpm7* Embryonic Defects with Divalent-Cation Supplementation

Mg^{2+} and Ca^{2+} supplementation differentially rescued melanophore and touch-response phenotypes of *tct*^{b508} embryos. High concentrations of $CaCl_2$ were toxic at normal NaCl concentrations ("0" in the figure), although embryo viability could be restored at lower NaCl concentrations ("−" in the figure).

(A) Mean ± standard error of the mean (SEM) proportion of *trpm7*^{b508} embryos exhibiting rescued melanophores (as in Figure 1F in the main text). In the standard embryo medium (solution A) and the reduced-NaCl rearing medium (B), no embryos exhibited rescued melanophores. In the medium with supplementary $MgCl_2$ (100 mM; solutions C and D), many embryos exhibited partial melanophore rescue. Although melanophore rescue was not observed in the medium containing low supplementary $CaCl_2$ (50 mM) without $MgCl_2$ (solution E), partial rescue occurred in media containing high supplementary $CaCl_2$ (100 mM) without $MgCl_2$ supplementation (solution F) or low $CaCl_2$ (50 mM) with high $MgCl_2$ (100 mM; solution G).

(B) Mean ± SEM proportion of *trpm7*^{b508} embryos exhibiting touch response. In contrast to melanophore rescue, touch response was not rescued by $MgCl_2$ supplementation alone (solutions C and D). Rather, touch response was maximally rescued with low supplementary $CaCl_2$ (50 mM) without $MgCl_2$ (solution E), although some rescue also occurred with higher $CaCl_2$ (100 mM) supplementation (solution F) or with low $CaCl_2$ (50 mM) in the presence of $MgCl_2$ (100 mM; solution G). Qualitatively similar responses to $CaCl_2$ and $MgCl_2$ supplementation also were observed with *trpm7*^{j124e2} (*nutria*), which exhibit a weaker embryonic melanophore phenotype than *trpm7*^{b508}. The same media did not rescue similar melanophore defects of *sparse* (*kit*) or *colorless* (*sox10*) mutants [S12, S13], demonstrating specificity of the effect for *trpm7* (data not shown). The cellular basis of the touch phenotype is unclear. Because of the timing and recovery of this phenotype, it is unlikely to depend on hair cells of lateral-line neuromasts, recently shown to require TRP family members NompC and TRPA1 [S14, S15]. Toxicity of high-salt solutions precluded testing for rescue of later, larval ossification phenotypes.

experimental study of intraspecific variation, developmental timing, and heterochrony in fishes. Evolution Int. J. Org. Evolution 54, 2091–2106.

S9. Storey, J.D., and Tibshirani, R. (2003). Statistical significance for genomewide studies. Proc. Natl. Acad. Sci. USA 100, 9440–9445.

S10. Cornell, R.A., Yemm, E., Bonde, G., Li, W., d'Alencon, C., Wegman, L., Eisen, J., and Zahs, A. (2004). Touchtone promotes survival of embryonic melanophores in zebrafish. Mech. Dev. 121, 1365–1376.

S11. Arduini, B.L., and Henion, P.D. (2004). Melanophore sublineage-specific requirement for zebrafish touchtone during neural crest development. Mech. Dev. 121, 1353–1364.

S12. Parichy, D.M., Rawls, J.F., Pratt, S.J., Whitfield, T.T., and Johnson, S.L. (1999). Zebrafish *sparse* corresponds to an orthologue of c-*kit* and is required for the morphogenesis of a subpopulation of melanocytes, but is not essential for hematopoiesis or primordial germ cell development. Development 126, 3425–3436.

S13. Dutton, K.A., Pauliny, A., Lopes, S.S., Elworthy, S., Carney, T.J., Rauch, J., Geisler, R., Haffter, P., and Kelsh, R.N. (2001). Zebrafish *colourless* encodes sox10 and specifies non-ectomesenchymal neural crest fates. Development 128, 4113–4125.

S14. Sidi, S., Friedrich, R.W., and Nicolson, T. (2003). NompC TRP channel required for vertebrate sensory hair cell mechanotransduction. Science 301, 96–99.

S15. Corey, D.P., Garcia-Anoveros, J., Holt, J.R., Kwan, K.Y., Lin, S.Y., Vollrath, M.A., Amalfitano, A., Cheung, E.L., Derfler, B.H., Duggan, A., et al. (2004). TRPA1 is a candidate for the mechanosensitive transduction channel of vertebrate hair cells. Nature 432, 723–730.

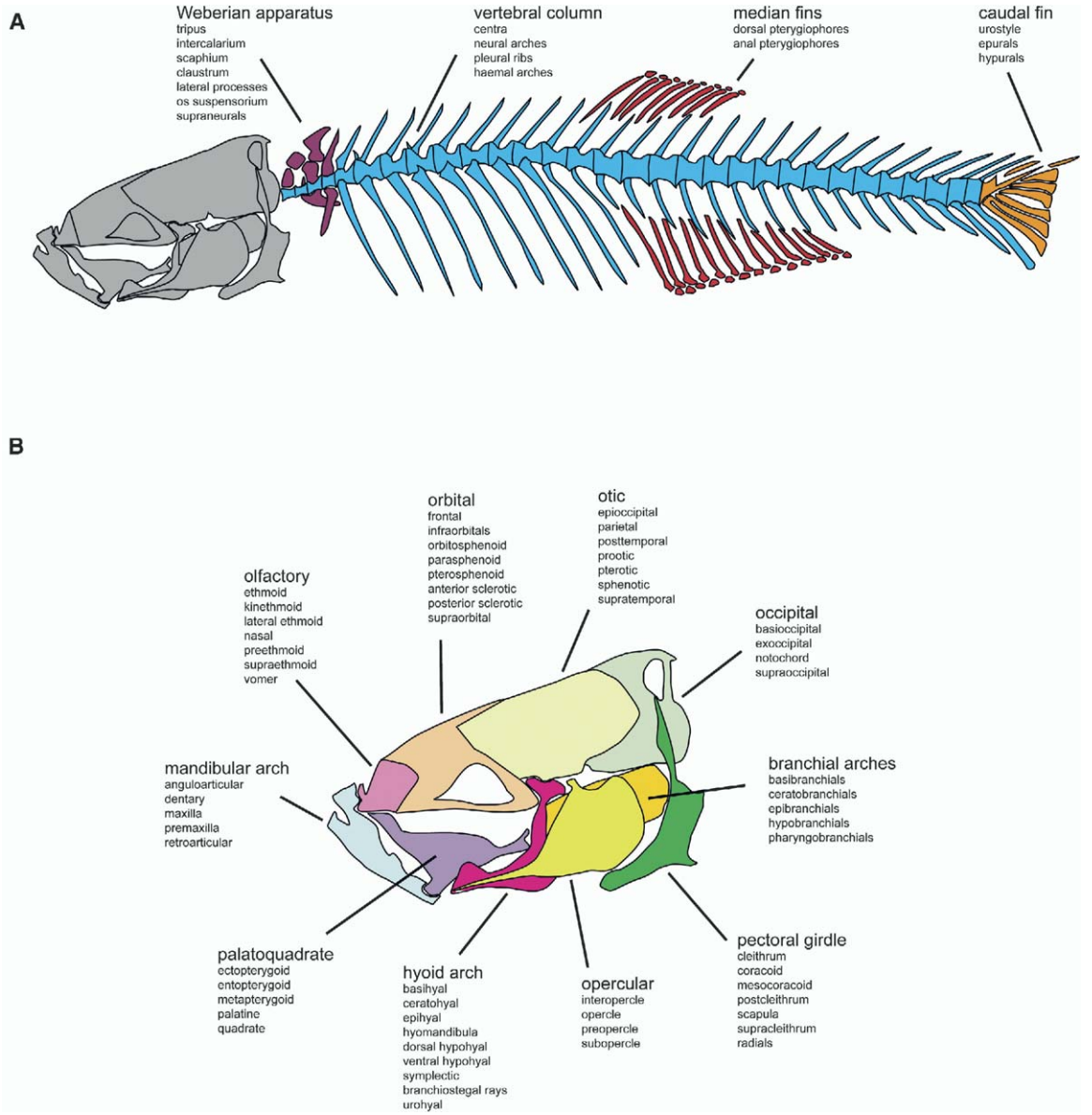

Figure S3. Functional-Anatomical Units and Bone Locations Examined for Ossification Sequence and Timing

Functional-anatomical units are color coded to match Figures 4A–4C in the main text. (A) shows units of the postcranial skeleton with bones comprising these units listed in small type. (B) shows units and bones of the craniofacial skeleton.

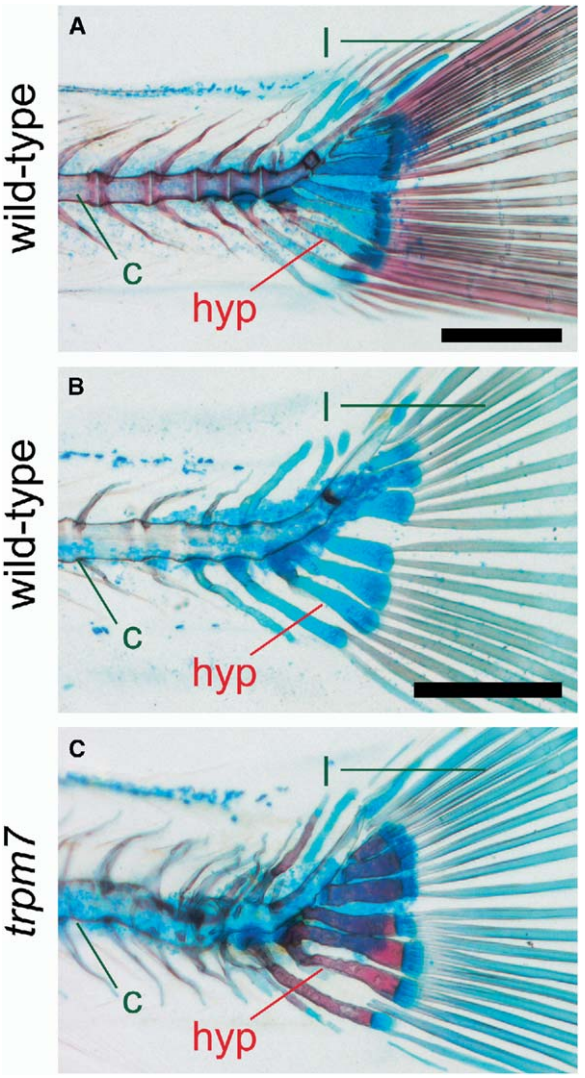

Figure S4. Growth Retardation Alone Does Not Result in Precocious Ossification

Three siblings from a cross segregating *trpm7*^{j124e2}.

(A) Wild-type fish showing endochondral hypurals (denoted by "hyp") that are not yet ossified, as well as intramembranous vertebral centra (denoted by "c") and fin lepidotrichia (denoted by "l") that are already well ossified.

(B) Even severely runted wild-type individuals that are from the same family and are indistinguishable in size from *trpm7* mutants do not show precocious ossification of endochondral hypurals (or other bones); the ossification of intramembranous centra and lepidotrichia is delayed, reflecting an overall retardation of developmental rate in slow-growing fish.

(C) *trpm7* mutant has accelerated hypural ossification and delayed centra and lepidotrichial ossification compared to wild-type. In contrast to runted wild-type individuals, delayed ossification of intramembranous bones does not reflect a general developmental retardation because the absolute timing of other events (cartilage formation, chondrocyte and osteoblast appearance, adult pigment-pattern formation, gut looping, swim-bladder bifurcation, etc.) does not differ dramatically from wild-type.

Scale bars represent (A), 400 μm and (B and C), 400 μm.

Table S1. Relative Ossification Timing

Endochondral Bones

Bone	Group[a]	Effect ± SEM[b]	χ^2	*P*[c]	s[d]
anal pterygiophores	medial fins	−2.82 ± 0.219	166.13	0	***
basibranchial 1	branchial arches	−0.97 ± 0.128	57.71	3.0E-14	***
basibranchial 2	branchial arches	−1.86 ± 0.148	159.00	0	***
basibranchial 3	branchial arches	−0.80 ± 0.150	28.42	9.8E-08	***
basihyal	hyoid	−1.84 ± 0.130	200.44	0	***
basioccipital	occipital	−0.02 ± 0.148	0.02	0.9	NS
basipterygium	pelvic girdle	−0.20 ± 0.146	1.94	0.2	NS
ceratobranchial 1	branchial arches	−0.88 ± 0.091	93.59	0	***
ceratobranchial 2	branchial arches	−0.74 ± 0.088	70.04	1.1E-16	***
ceratobranchial 3	branchial arches	−0.62 ± 0.087	50.30	1.3E-12	***
ceratobranchial 4	branchial arches	−0.57 ± 0.099	33.37	7.6E-09	***
ceratobranchial 5	branchial arches	0.40 ± 0.136	8.62	0.003	*
ceratohyal	hyoid	−0.67 ± 0.092	53.45	2.7E-13	***
claustrum	Weberian	0.23 ± 0.112	4.16	0.04	NS
coracoid	pectoral girdle	−0.11 ± 0.097	1.36	0.2	NS
dorsal hypohyal	hyoid	0.17 ± 0.130	1.73	0.2	NS
dorsal pterygiophores	medial fins	−2.63 ± 0.209	157.18	0	***
epibranchial	branchial	−1.12 ± 0.096	135.88	0	***
epihyal	hyoid	−0.28 ± 0.094	8.99	0.003	*
epioccipital	otic	−0.28 ± 0.095	8.60	0.003	*
epurals	caudal fin	−4.67 ± 0.386	145.86	0	***
ethmoid	olfactory	1.04 ± 0.380	7.51	6.1E-03	*
exoccipital	occipital	0.07 ± 0.129	0.28	0.6	NS
haemal arches	vertebral	0.35 ± 0.105	10.86	9.8E-04	*
hyomandibula	hyoid	−0.59 ± 0.110	28.50	9.4E-08	***
hypurals	caudal fin	−0.66 ± 0.088	55.60	8.9E-14	***
kinethmoid	olfactory	0.21 ± 0.103	4.22	0.04	NS
lateral ethmoid	olfactory	−0.56 ± 0.088	39.93	2.6E-10	***
mesocoracoid	pectoral girdle	0.26 ± 0.124	4.49	0.03	NS
metapterygoid	palatoquadrate	−1.48 ± 0.119	154.06	0	***
orbitosphenoid	orbital	0.05 ± 0.103	0.24	0.6	NS
os suspensorium	Weberian	0.06 ± 0.129	0.19	0.7	NS
palatine	palatoquadrate	−0.10 ± 0.092	1.28	0.3	NS
pectoral radials	pectoral girdle	−0.20 ± 0.122	2.64	0.1	NS
pharyngobranchial	branchial arches	−2.17 ± 0.510	18.06	2.1E-05	***
prootic	otic	−0.28 ± 0.137	4.18	0.04	NS
pterosphenoid	orbital	−0.05 ± 0.089	0.31	0.6	NS
pterotic	otic	0.04 ± 0.083	0.28	0.6	NS
quadrate	palatoquadrate	−0.52 ± 0.096	29.39	5.9E-08	***
retroarticular	mandibular	−0.05 ± 0.085	0.28	0.6	NS
scaphium	Weberian	0.17 ± 0.082	4.08	0.04	NS
scapula	pectoral girdle	−0.07 ± 0.105	0.41	0.5	NS
sphenotic	otic	−0.50 ± 0.085	34.26	4.8E-09	***
supraneurals	Weberian	−0.20 ± 0.085	5.57	0.02	*
supraoccipital	occipital	−0.88 ± 0.106	69.74	1.1E-16	***
symplectic	hyoid	−1.12 ± 0.093	147.16	0	***
tripus	Weberian	0.06 ± 0.129	0.24	0.6	NS
ventral hypohyal	hyoid	−0.21 ± 0.090	5.69	0.02	*

Intramembranous Bones

Bone	Group	Effect ± SEM	χ^2	*P*	s
anguloarticular	mandibular	−0.12 ± 0.087	2.01	0.2	NS
branchiostegal rays	hyoid	0.20 ± 0.101	3.97	0.05	NS
centra W[e]	vertebral	0.64 ± 0.158	16.20	5.7E-05	***
centra c	vertebral	0.42 ± 0.104	15.91	6.6E-05	***
centra pre-c	vertebral	−0.05 ± 0.114	0.17	0.7	NS
cleithrum	pectoral girdle	0.36 ± 0.129	7.60	0.006	*
dentary	mandibular	−0.17 ± 0.115	2.05	0.2	NS
ectopterygoid	palatoquadrate	0.87 ± 0.181	23.31	1.4E-06	***
entopterygoid	palatoquadrate	0.34 ± 0.080	17.66	2.6E-05	***
frontal	orbital	0.83 ± 0.201	17.07	3.6E-05	***
infraorbitals	orbital	1.23 ± 0.308	15.62	7.7E-05	***
interopercle	opercular	0.27 ± 0.088	9.10	0.003	*
lateral processes	Weberian	0.13 ± 0.130	0.96	0.3	NS

(continued)

Table S1. Continued

Intramembranous Bones

Bone	Group	Effect ± SEM	χ^2	*P*	s
maxilla	mandibular	0.48 ± 0.107	20.10	7.4E-06	***
nasal	olfactory	1.22 ± 0.374	10.57	0.001	*
neural arches c	vertebral	0.36 ± 0.108	11.24	8.0E-04	*
neural arches pre-c	vertebral	−0.12 ± 0.123	0.95	0.3	NS
notochord	occipital	0.25 ± 0.137	3.25	0.07	NS
opercle	opercular	−0.07 ± 0.122	0.31	0.6	NS
parasphenoid	orbital	0.18 ± 0.102	3.02	8.2E-02	NS
parietal	otic	−0.05 ± 0.709	0.01	0.9	NS
pleural ribs	vertebral	−0.01 ± 0.129	0.01	1	NS
postcleithrum	pectoral girdle	0.44 ± 0.135	10.49	0.001	*
posttemporal	otic	−0.14 ± 0.093	2.24	0.1	NS
premaxilla	mandibular	0.47 ± 0.104	20.15	7.2E-06	***
preopercle	opercular	0.31 ± 0.085	13.62	2.2E-04	**
subopercle	opercular	0.92 ± 0.092	101.24	0	***
supracleithrum	pectoral girdle	0.40 ± 0.128	9.90	0.002	*
supraethmoid	olfactory	0.77 ± 0.174	19.56	9.8E-06	***
supraorbital	orbital	1.15 ± 0.241	22.82	1.8E-06	***
urohyal	hyoid	−0.01 ± 0.089	0.01	0.9	NS
urostyle	caudal fin	0.96 ± 0.112	73.46	0	***
vomer	olfactory	0.67 ± 0.155	18.30	1.9E-05	***

[a] Functional-anatomical grouping.

[b] Partial logistic regression coefficient: relative likelihood of bone being ossified in wild-type as compared to mutant (negative values reflect precocious ossification in mutant; positive values reflect delayed ossification in mutant).

[c] Probability that effect differs significantly from 0 (χ^2, 1 d.f.).

[d] Significance of effect after controlling for multiple comparisons (q, significance level controlled by false-discovery-rate method; a, significance level controlled by Bonferroni method; see main article text). NS = not significant. *: $q < 0.01$, $a > 0.05$. **: $q < 0.01$, $a < 0.05$. ***: $q < 0.01$, $a < 0.01$.

[e] The following abbreviations are used: W, Weberian; c, caudal; pre-c, pre-caudal.